

(g) Mode 7 [$t_6 \leq t < t_7$]

Figure 5: (Continued).

2.2 With an Active Snubber

The operation of the interleaved buck converter with an active snubber over one switching cycle can be divided into seven major operating modes. The driving signals, current and voltage waveforms of its key components are shown in Fig. 6. Fig. 7 shows the equivalent circuit modes of the interleaved buck converter with an active snubber over a switching cycle.

1). Mode 1 [Fig. 7(a), $t_0 \leq t < t_1$]:

In this mode, main switch M_1 continuously turned on and auxiliary switch M_{22} is turned on to create a ZVS condition. The capacitor C_{r2} begins releasing its stored energy through M_{22} , L_{r2} and L_{22} . At this interval, coupled inductors L_2 and L_{22} are discharged continuously to the load.

2). Mode 2 [Fig. 7(b), $t_1 \leq t < t_2$]:

At time t_1 , main switch M_1 is turned off, and auxiliary switch M_{11} and free-wheeling diode D_1 still stay in the off state. During this interval, main switch M_2 maintains in the off state, while auxiliary M_{22} as well as free-wheeling diode D_2 still stay in the on-state. In this mode, resonant inductor L_{r1} releases its energy to stray capacitance C_{M1} of M_1 and stray capacitance C_{M11} of M_{11} with a resonant manner. Stray capacitance C_{M1} of M_1 is charged toward $(V_i + nV_o)$ while stray capacitance C_{M11} of M_{11} is discharged down to zero. To achieve a ZVS feature for switch M_{11} , the energy stored in resonant inductor L_{r1} should satisfy the following inequality:

$$0.5 \times [i_{DS1}(t_1)]^2 L_{r1} \geq 0.5 \times [V_{DS11}(t_1)]^2 (C_{M1} // C_{M11}). \quad (13)$$

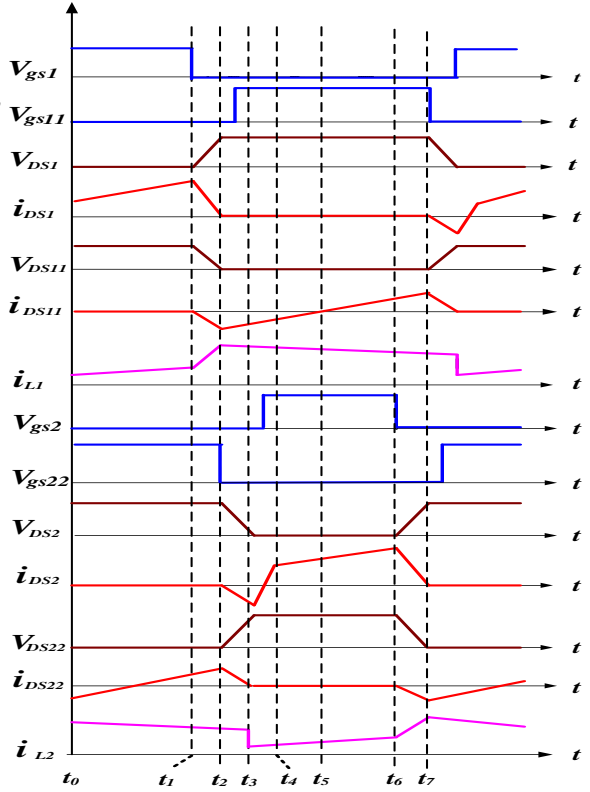


Figure 6: Key waveforms of interleaved buck converter with an active snubber.

3). Mode 3 [Fig. 7(c), $t_2 \leq t < t_3$]:

Mode 3 begins when voltage V_{DS11} of M_{11} reaches zero at t_2 . Current i_{DS11} forces the body diode D_{M11} of M_{11} conducting and creating a ZVS condition for M_{11} . The driving signal is applied to switch M_{11} when its body diode is conducting and achieving a ZVS feature. In this mode, voltage V_{DS1} of M_1 increases continuously, and then V_{DS1} of M_1 is clamped to $V_{in} + V_{Cr1}$. Meanwhile, free-wheeling diode D_1 begins conducting. Coupled Inductors L_1 and L_{11} are discharged through free-wheeling diode D_1 to the load. The currents of the inductors can be expressed as follows:

$$i_{L1}(t) = \frac{V_o}{nL_1} \times (t - t_2) + i_{L1}(t_2), \quad (14)$$

and

$$i_{L2}(t) = \frac{V_o}{nL_2} \times (t - t_2) + i_{L2}(t_2). \quad (15)$$

The energy trapped in the resonant inductor L_{r1} is recycled to clamp capacitor C_{r1} . Due to the clamp capacitance of C_{r1} being large enough, voltage V_{Cr1} will keep constant.

In this mode, when auxiliary switch M_{22} is turned off at time t_3 , resonant inductor L_{r2} resonates with C_{M2} and C_{M22} . Stray capacitance C_{M22} of M_{22} is continuously charged toward $V_{Cr2} + [n/(1+n)](V_i - V_o)$, while stray capacitance C_{M2} of M_2 is discharged down to zero. To achieve a ZVS feature for switch M_2 , the energy trapped in resonant inductor L_{r2} should satisfy the following inequality:

$$0.5 \times [i_{DS2}(t_2)]^2 L_{r2} \geq 0.5 \times [V_{DS2}(t_2)]^2 (C_{M2} // C_{M22}). \quad (16)$$

4). Mode 4 [Fig. 7(d), $t_3 \leq t < t_4$]:

Mode 4 begins when voltage V_{DS2} of M_2 drops to zero at t_3 . Current i_{DS2} forces the body diode D_{M2} of M_2 conducting and creating a ZVS condition for M_2 . The driving signal is applied to switch M_2 when its body diode is conducting and achieving a ZVS feature.

5). Mode 5 [Fig. 7(e), $t_4 \leq t < t_5$]:

At time t_4 , main switch M_2 is turned on, and auxiliary switch M_{22} and free-wheeling diode D_2 are in the off states. Current i_{L2} flows through the path of $V_i - L_{22} - L_{r2} - M_2 - L_2 - V_o$, and inductor current i_{L1} continuously flows through the path of $V_o - D_1 - L_1$. Inductor current i_{L2} linearly increases, and i_{L1} linearly decreases, which can be expressed as follows:

$$i_{L1}(t) = \frac{V_o}{nL_1} \times (t - t_4) + i_{L1}(t_4), \quad (17)$$

and

$$i_{L2}(t) = \frac{V_i - V_o}{n^2 L_2} \times (t - t_4) + i_{L2}(t_4). \quad (18)$$

6). Mode 6 [Fig. 7(f), $t_5 \leq t < t_6$]:

At time t_5 , main switch M_2 is turned off, and auxiliary switch M_{22} and free-wheeling diode D_2 still stay in the off state. During this interval, main switch M_1 maintains in the off state, while auxiliary M_{11} as well as free-wheeling diode D_1 still stay in the on states. In this mode, resonant inductor L_{r2} releases its energy to stray capacitance C_{M2} of M_2 and stray capacitance C_{M22} of M_{22} with a resonant manner. Stray capacitance C_{M2} is charged toward $(V_i + nV_o)$, while stray capacitance C_{M22} is discharged down to zero. To achieve a ZVS feature for switch M_{22} , the energy stored in resonant inductor L_{r2} should satisfy the following inequality:

$$0.5 \times [i_{DS2}(t_5)]^2 L_{r2} \geq 0.5 \times [V_{DS11}(t_5)]^2 (C_{M2} // C_{M22}). \quad (19)$$

7). Mode 7 [Fig. 7(g), $t_6 \leq t < t_7$]:

Mode 7 begins when voltage V_{DS22} of M_{22} reaches zero at t_8 . Current i_{DS22} forces the body diode D_{M22} of M_{22} conducting and creating a ZVS condition for M_{22} . The driving signal should be applied to switch M_{22} when its body diode is conducting and achieving a ZVS feature. In this mode, voltage V_{DS2} increases continuously, and then V_{DS2} of M_2 is clamped to $V_i + V_{Cr2}$. Meanwhile, free-wheeling diode D_2 begins conducting. Coupled inductors L_2 and L_{22} are discharged through free-wheeling diode D_2 to the load. The currents of the inductors can be expressed as follows:

$$i_{L1}(t) = \frac{V_o}{nL_1} \times (t - t_6) + i_{L1}(t_6), \quad (20)$$

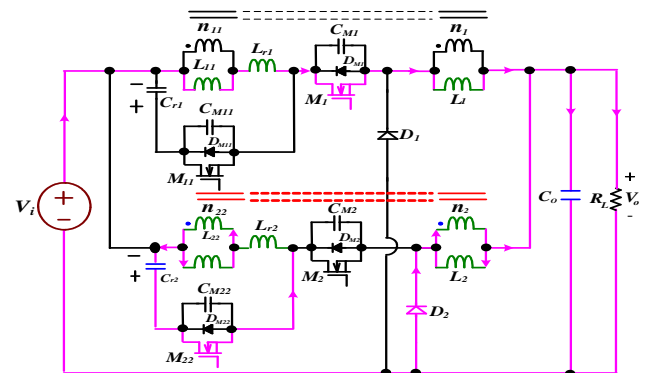
and

$$i_{L2}(t) = \frac{V_o}{nL_2} \times (t - t_6) + i_{L2}(t_6). \quad (21)$$

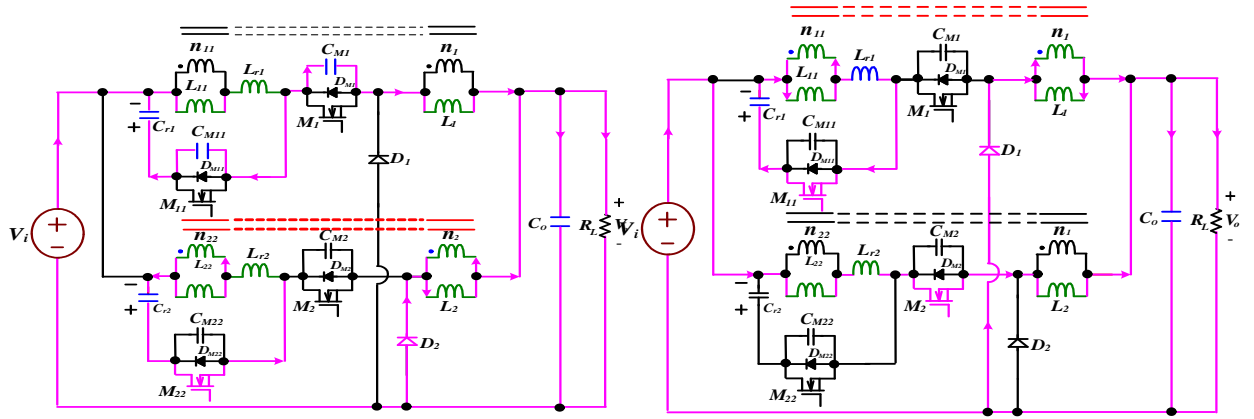
The energy trapped in the resonant inductor L_{r2} is recycled to clamp capacitor C_{r2} . Since the clamp capacitor C_{r2} is large enough, voltage V_{Cr2} will keep constant. In order to achieve a ZVS feature for switch M_1 , the energy stored in resonant inductor L_{r1} should satisfy the following inequality:

$$0.5 \times [i_{DS1}(t_6)]^2 L_{r1} \geq 0.5 \times [V_{DS1}(t_6)]^2 (C_{M1} // C_{M11}). \quad (22)$$

When the main switch M_1 starts conducting again at the end of mode 7, the converter operation over one switching cycle is completed.

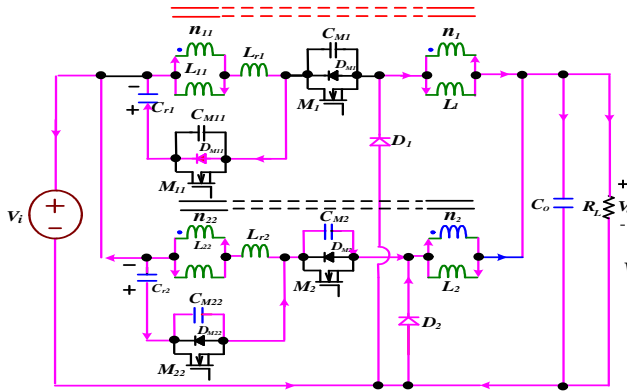


(a) Mode 1 [$t_0 \leq t < t_1$]

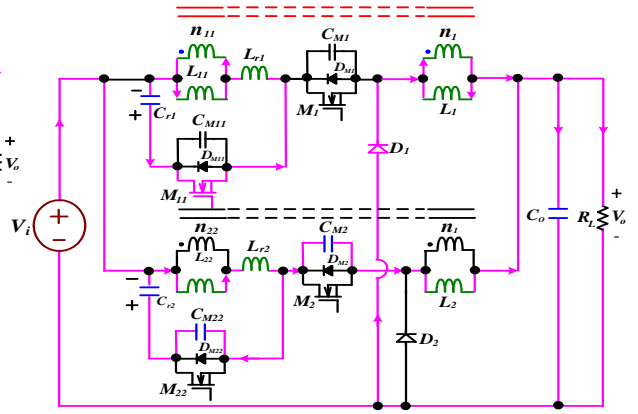


(b) Mode 2 $[t_1 \leq t < t_2]$

(e) Mode 5 $[t_4 \leq t < t_5]$

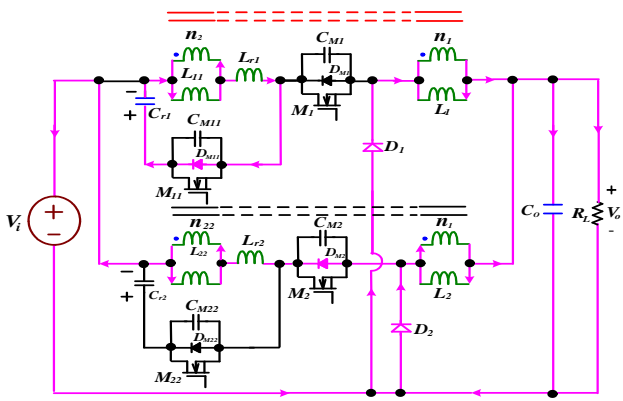


(c) Mode 3 $[t_2 \leq t < t_3]$

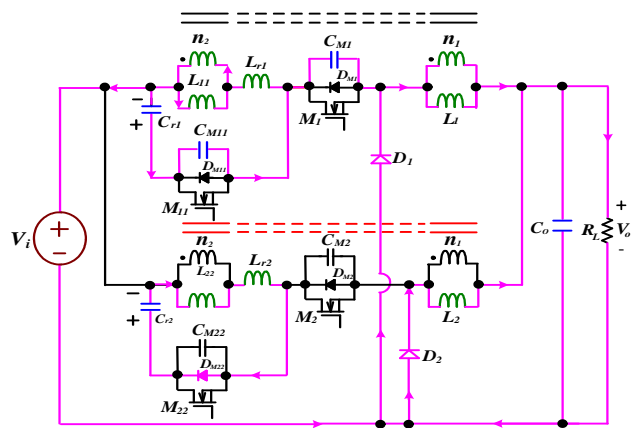


(f) Mode 6 $[t_5 \leq t < t_6]$

Figure 7: Equivalent circuit modes of interleaved buck converter with an active snubber.



(d) Mode 4 $[t_3 \leq t < t_4]$



(g) Mode 7 $[t_6 \leq t < t_7]$

Figure 7: (Continued).

3. Comparison Between Two Different Snubbers

Soft-switching methods usually add snubbers to the original interleaved buck converter to reduce switching losses. This section presents comparison between two different snubbers of the interleaved buck converters. The features of two different snubbers are described as follows:

3.1 Features of the Passive Snubber

In Fig. 1, the interleaved buck converter with the passive snubber has the advantages as follows: 1) It can achieve zero-voltage-transition (ZVT) under turn-off condition. Therefore, the turn-off switching losses of active switches can be substantially reduced. 2) The passive snubber needs only passive components such as diodes and capacitors, which have simple structures and low cost. However, the interleaved buck converter with a passive snubber has disadvantages. For example, the active switches are operated at hard-switching during turn-on transition. As a result, turn-on losses and EMI conditions are significant. Additionally, the passive snubber usually requires many passive components that might increase the complexity of printed circuit board (PCB) layout.

3.2 Features of the Active Snubber

In Fig. 2, the interleaved buck converter with the active snubber has the advantages as follows: 1) It can achieve ZVS feature under turn-on condition and ZVT feature under turn-off condition. Therefore, the switching losses at turn-on transition can be completely removed, and conversion efficiency can be further increased. 2) It can be operated at high frequency, reducing converter size, and EMI. However, the interleaved buck converter with an active snubber has disadvantages. For example, extra active switches and resonant inductor result in complex control.

To objectively judge the merits of two snubbers, the interleaved buck converter with a passive and an active snubber is shown in Table 1.

Table 1: Comparison between the features of two different snubbers in the interleaved buck converters.

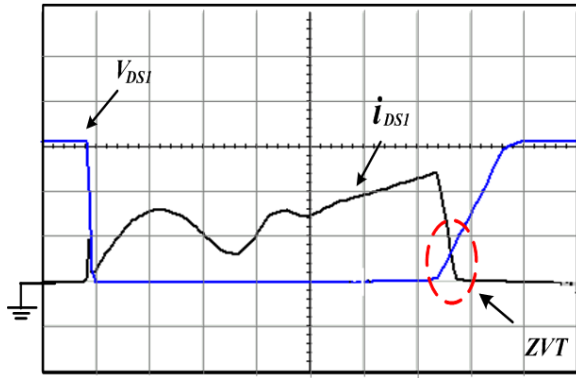
	with a passive snubber (in Fig. 1)	with an active snubber(in Fig. 2)
soft-switching feature of active switches	<ul style="list-style-type: none"> ● hard-switching turn-on ● ZVT turn-off 	<ul style="list-style-type: none"> ● ZVS turn-on ● ZVT turn-off
component counts	● many components	● less components
power losses	● large	● small
control circuit	● easy	● difficult

4. Experimental Results

In order to compare the features between two different snubbers in the interleaved buck converter, a 240W prototype of the interleaved buck converter was built. The specifications are listed again as follows:

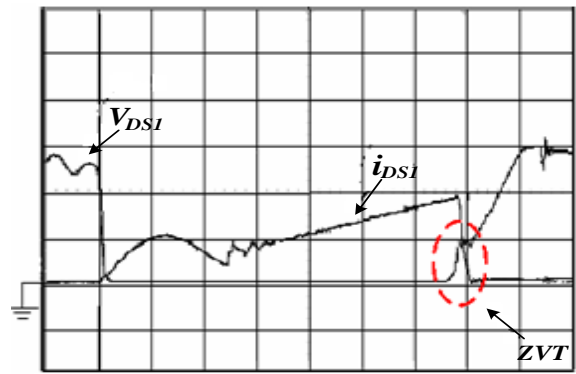
- input voltage: 150-200 V_{dc},
- output voltage: 12 V_{dc},
- output current: 20 A, and
- switching frequency: 75 kHz.

Fig. 8 shows simulated and experimental voltage and current waveforms of the active switches at turn-off transitions for an interleaved buck converter with a passive snubber. From Fig. 8, it can be seen that the active switches have ZVT features. However, it has switching overlap of voltage and current resulting in low switching losses at turn-off transitions. Fig. 9 shows simulated and experimental voltage and current waveforms of the active switches for interleaved buck converter with an active snubber. From Fig. 9, it can be seen that the active switches have ZVS features, and there is not any switching losses at turn-off transitions. Therefore, it has high conversion efficiency and low EMI. Fig. 10 shows efficiency measurements of the interleaved buck converter with a passive snubber and an active snubber. Fig. 10 shows efficiency comparison between two snubbers. It can be seen that the conversion efficiency of an interleaved buck converter with an active snubber can reach 89% under full load condition. This reason is that the active switches have ZVS features, which result in that the switching losses at turn-on transition high efficiency.



(V_{DS} : 100V/div, i_{DS} : 5A/div, Time: 1 μ s/div)

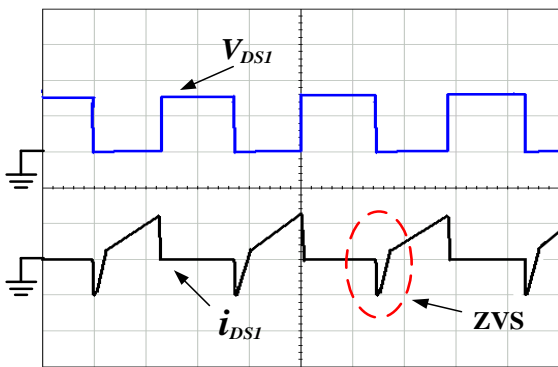
(a)



(V_{DS} : 100V/div, i_{DS} : 5A/div, Time: 1 μ s/div)

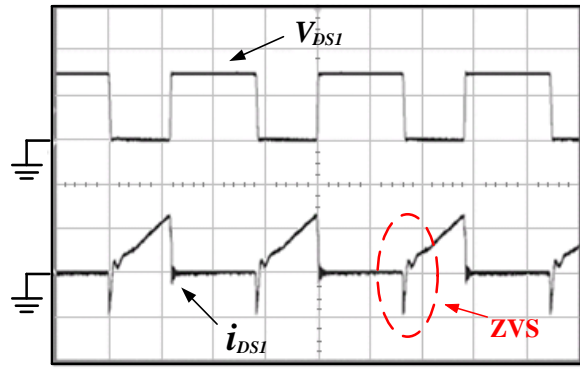
(b)

Figure 8: Voltage and current waveforms of the active switches with a passive snubber: (a) simulated result, (b) experimental result.



(V_{DSII} : 200 V/div; i_{DSII} : 10 A/div; Time: 5 μ s/div)

(a)



(V_{DSII} : 200 V/div; i_{DSII} : 10 A/div; Time: 5 μ s/div)

(b)

Figure 9: Voltage and current waveforms of the active switches with an active snubber: (a) simulated result, (b) experimental result.

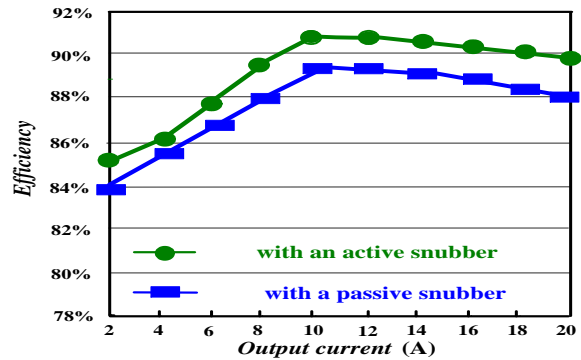


Figure 10: Plots of efficiency versus output current for the interleaved buck converter with a passive and an active snubber under full-load condition.

5. Conclusions

In this paper, the comparison between two different snubbers of an interleaved buck converter has been implemented. The interleaved buck converter with a passive snubber has disadvantages. For example, the active switches are operated at hard-switching during turn-on transition. As a result, turn-on losses and EMI conditions are significant. The interleaved buck converter with an active snubber has the advantages. For example, it can achieve ZVS and ZVT features, resulting in low EMI and high efficiency. For the requirements of high power density, high efficiency and low power losses, the interleaved buck converter with an active snubber is relatively attracted.

References

- [1]. Ilic, M. and Maksimovic, D., "Interleaved zero-current-transition buck converter," IEEE Trans. Ind. Appl., Vol. 43, 2007, pp.1619–1627.
- [2]. M. Xu, J. Zhou, and F. C. Lee, "A Current-Triple DC/DC Converter," IEEE Trans. on Power Electronics, Vol. 19, Issue: 3, 2004, pp. 693 – 700.
- [3]. Tsai, C.-T.; Shen, C.-L., "High step-down interleaved buck converter with active-clamp circuits for wind turbines," Energies Vol. 5, 2012, pp. 5150–5170.
- [4]. M. Xu, J. Zhou, and F. C. Lee, "A Current-Triple DC/DC Converter," IEEE Trans. on Power Electronics, Vol. 19, 2004, pp. 693 – 700.
- [5]. J. A. Abu-Qahouq, H. Mao and I. Batarseh, "New Coupled-Inductors Current-Doubler Topology," Proceedings of Power Electronics Specialists Conference, Vol. 2, 2003, pp. 648-655.
- [6]. A. Pietkiewicz and D. Tollik, "Coupled-Inductor Current-Doubler Topology in Phase-Shift Full-Bridge DC-DC Converter," Proceedings of Telecommunications Energy Conference, 1998, pp. 41-48.
- [7]. Tsai-Fu Wu, et al., "Analysis and Implementation of an Improved Current-Doubler Rectifier with Coupled Inductors," IEEE Trans. on Power Electronics, Vol. 23, 2008, pp. 2681-2693.
- [8]. Chen, Y. M., Tseng, S. Y., Tsai, C.T. and Wu, T. F. Interleaved buck converters with a single-capacitor turn-off snubber. IEEE Trans. Aerosp. Electron. Syst. Vol. 40, 2004, pp. 954–967.
- [9]. Shen-Yaur Chen and Jin-Jia Chen, "Study of the Effect and Design Criteria of the Input Filter for Buck Converters with Peak Current-Mode Control Using a Novel System Block Diagram," IEEE Transactions on Industrial Electronics, Vol. 55, 2008, pp. 3159–3166.
- [10]. N. P. Papanikolaou and E. C. Tatakis, "Active voltage clamp in flyback converters operating in CCM mode under wide load variation," IEEE Trans. Ind. Electron., vol. 51, 2004, pp. 632–640.
- [11]. Chu-Yi Chiang and Chern-Lin Chen, "Zero-Voltage-Switching Control for a PWM Buck Converter under DCM/CCM Boundary," IEEE Transactions on Power Electronics, Vol. 24, 2009, pp. 2120–2126.
- [12]. L. S. Yang, T. J. Liang, H. C. Lee, and J. F. Chen, "Novel high step up dc–dc converter with coupled-inductor and voltage-doubler circuits," IEEE Trans. Ind. Electron., Vol. 58, 2011, pp. 4196–4206.
- [13]. T. F. Wu, Y. S. Lai, J. C. Hung, and Y. M. Chen, "Boost converter with coupled inductors and buck–boost type of active clamp," IEEE Trans. Ind. Electron., Vol. 55, 2008, pp. 154–162.
- [14]. A. Hren, J. Korelic, and M. Milanovic, "RC-RCD clamp circuit for ringing losses reduction in a flyback converter," IEEE Trans. Circuits Syst. II, Vol. 53, 2006, pp. 369–373.



Cheng-Tao Tsai received the B.S. degree in electrical engineering in 1991 from Feng Chia University, Taichung, Taiwan, and the M.S. and Ph.D. degree from the National Chung Cheng University, Chia-Yi, Taiwan, in 2003 and 2008,

respectively. In 2009, he joined the National Chin-Yi University of Technology, Taichung, Taiwan, where he is currently an Associate Professor in the Department of Electrical Engineering. His current research interests include design of switching-mode power supplies, power factor correction technology, and chargers for electric vehicles.



Ying-Che Kuo received the B.S. and M.S. degree in automatic control engineering from Feng Chia University, Taichung, Taiwan, in 1986 and 1988 respectively, and the Ph.D. degree in institute of communications engineering

from the National Chiao Tung University, Hsinchu, Taiwan, in 2005. In 1990, he joined the National Chin-Yi University of Technology, Taichung, Taiwan, where he is currently an Associate Professor in the Department of Electrical Engineering. His current research interests focus on intelligent vehicle, image processing and analysis, and application of embedded system.



Ying-Piao Kuo received the B.S. degree in electrical engineering in 1985 from the National Taiwan University of Science and Technology, Taipei, Taiwan, and the M.S. degree in electrical engineering in 1989

from the National Taiwan University, and Ph.D. degree from the National Taiwan University of Science and Technology, Taipei, Taiwan, in 2011. In 1989 he joined the National Chin-Yi University of Technology, Taichung, Taiwan, where he is currently an Associate Professor in the Department of Electrical Engineering. His current research interests include design of switching-mode power supplies, partial discharge and power system stability.



Yung-Chang Luo received the M.S. and Ph.D. degree from the National Taiwan University of Science and Technology, Taipei, Taiwan, in 1991 and 2000, respectively. Currently, he is an Associate Professor at the

Department of Electrical Engineering, National Chin-Yi University of Technology, Taichung, Taiwan. His research interests include speed-sensorless ac motor drives, front-end power factor correction of converter, and design of micro-controller-based motor drive.